

# Global model of inductively coupled Ar plasmas using two-temperature approximation

T. Kimura and K. Ohe

*Department of Systems Engineering, Nagoya Institute of Technology, Nagoya 466-8555, Japan*

(Received 6 November 2000; accepted for publication 18 January 2001)

The electron energy distribution function (EEDF) is measured with a Langmuir probe in an inductively coupled rf (13.56 MHz) Ar discharge in the pressure range from 5 to 70 mTorr, by changing the power injected into the plasma up to 100 W. The EEDFs measured at a pressure of 5 mTorr formed a bi-Maxwellian structure, which is not prominent due to high electron density, in the energy region lower than the lowest excitation threshold energy. The EEDF structure in the energy region higher than the threshold has a significant depletion of high energy electrons. The EEDF measured at a pressure higher than 10 mTorr can be approximated using a two-temperature distribution, which consists of the higher temperature in a low-energy region below the lowest excitation threshold and the lower temperature in a high-energy region. A global model using the two-temperature distribution is proposed and compared with the experimental results. The model consists of the rate equations for neutrals and charged particles and an energy-balance equation for electrons together with the balance equation for high-energy electrons. Pressure dependences of the electron density and temperatures predicted in this global model agree well with the experimental results except in the pressure range lower than 10 mTorr. © 2001 American Institute of Physics. [DOI: 10.1063/1.1354652]

## I. INTRODUCTION

Planar inductively coupled rf discharges operated at a pressure lower than 50 mTorr have been widely used for plasma processing, because they provide a simple way to produce a high-density plasma. Such a high density is achieved when the discharge is maintained by the azimuthal electric field induced by the rf coil current. The electron energy distribution function (EEDF) in inductively coupled discharges of various gases such as Ar, O<sub>2</sub>, and Ar/CF<sub>4</sub> have been measured in the electron density range of  $10^{16}$ – $10^{18}$  m<sup>-3</sup>.<sup>1–5</sup> The EEDF measured in Ar discharges at a pressure range lower than 5 mTorr formed a Maxwellian distribution except for the energy region lower than a few electron volts, whereas the electron energy probability function (EEPF) in the pressure higher than 5 mTorr formed a non-Maxwellian distribution due to the depletion of the energy higher than the lowest excitation threshold energy. The EEDFs in O<sub>2</sub> and Ar/CF<sub>4</sub> mixture discharges included a change from a Maxwellian-like distribution to a Druyvesteyn-like one with the increase of pressure.<sup>4,5</sup> These experimental results showed that the EEDF was mainly varied from a Maxwellian to a non-Maxwellian with a large depletion of the high energy region with increasing the pressure.

The study on modeling various discharge types is currently of great interest in understanding dependences of the plasma compositions and the electron kinetics on the external parameters. In many of these studies, time-dependent hydrodynamic models coupled to the Poisson equation and numerical methods such as Monte Carlo or particle in cell schemes are used in both capacitively and inductively coupled plasmas.<sup>6–8</sup> Moreover, the self-consistent electron

kinetic models,<sup>9,10</sup> which consist of the equations for the ion motion and the rf electric field induced from the external circuit, as well as the Boltzmann equation for electrons, can be also used for inductively coupled low-pressure rf Ar discharges under the assumption of the nonlocal electron kinetics. In the kinetic models, the spatial profiles of electron density, the plasma potential and ionization rate were described, indicating the formation of a non-Maxwellian EEDF which has a large depletion in the energy region higher than the lowest excitation threshold energy. Thus, the widely used Maxwellian EEDF assumption in the global model<sup>4,5,11–13</sup> for the high-density and low-pressure discharge, such as inductive rf plasma, may cause significant differences between the theoretical and experimental results of plasma parameters in the discharge volume.

The purpose of this article is to measure the pressure dependence of the EEDF in Ar inductively coupled discharges, and to compare with the global model using a two-temperature approximation of EEDF, in which the EEDF in the low-energy region below the lowest excitation threshold energy is represented as a truncated Maxwellian with the bulk temperature, and that in the high-energy region is by a Maxwellian tail with lower temperature. In Sec. II, we propose a global model using the two-temperature approximation of EEDF, in which the rate equations of the charged particle and the excited neutral species and the power balance equation for electrons together with the balance equation for high-energy electrons introduced to estimate the tail temperature are treated. In Sec. III, we briefly describe the experimental apparatus. In Sec. IV, the experimental results are compared with the present model. Section V presents concluding remarks.

TABLE I. Reactions included in the model.

No	Reaction	Rate coefficients ( $\text{m}^3 \text{s}^{-1}$ )	$q_j (\times 10^{-20} \text{m}^2)$	Ref.
1	$\text{Ar} + \text{e} \rightarrow \text{Ar}^m + \text{e}$	$k_1$	0.30	21
2	$\text{Ar} + \text{e} \rightarrow \text{Ar}^r + \text{e}$	$k_2$	0.50	21
3	$\text{Ar} + \text{e} \rightarrow \text{Ar}(4p + 4p') + \text{e}$	$k_3$	0.45	21
4	$\text{Ar} + \text{e} \rightarrow \text{Ar}(3d) + \text{e}$	$k_4$	1.20	21
5	$\text{Ar} + \text{e} \rightarrow \text{Ar}^+ + 2\text{e}$	$k_5$	3.15	21
6	$\text{Ar}^m + \text{e} \rightarrow \text{Ar}^+ + 2\text{e}$	$k_6 = 1.0 \times 10^{-13} \times \exp(-4.2/T_e)$		22
7	$\text{Ar}^r + \text{e} \rightarrow \text{Ar}^+ + 2\text{e}$	$k_7 = 1.0 \times 10^{-13} \times \exp(-4.2/T_e)$		22
8	$\text{Ar}^m + \text{e} \rightarrow \text{Ar}^r + \text{e}$	$k_8 = 2 \times 10^{-13}$		20
9	$\text{Ar}^m + \text{e} \rightarrow \text{Ar}^h + \text{e}$	$k_{mh}$		19,20
10	$\text{Ar}^r + \text{e} \rightarrow \text{Ar}^h + \text{e}$	$k_{rh}$		19,20
11	$\text{Ar}^r + \text{e} \rightarrow \text{Ar}^m + \text{e}$	$k_{11} = 3 \times 10^{-13}$		20
12	$\text{Ar}^m + \text{Ar}^m \rightarrow \text{Ar}^+ + \text{Ar} + \text{e}$	$k_{12} = 6 \times 10^{-16}$		20
13	$\text{Ar}^m + \text{Ar}^r \rightarrow \text{Ar}^+ + \text{Ar} + \text{e}$	$k_{13} = 2.10 \times 10^{-15}$		20
14	$\text{Ar}^r \rightarrow \text{Ar} + h\nu$	$\tau_{\text{rad}} = 2 \times 10^{-4} \text{ (s)}$		19
15	$\text{Ar}^h \rightarrow \text{Ar}^r + h\nu$	$\delta_{hr}$		19,20
16	$\text{Ar}^h \rightarrow \text{Ar}^m + h\nu$	$\delta_{hm}$		19,20
17	$\text{Ar}^m \rightarrow \text{Ar}$ (wall loss)	$D_m / \Lambda^2 (1/\Lambda^2 = (\pi/L)^2 + (2.405/R)^2)$		19,20
18	$\text{Ar}^+ \rightarrow \text{Ar}$ (wall loss)	$\text{Ar}_{\text{loss}}^+ = 2U_{B,\text{Ar}}(R^2 h_L + RLh_R)/R^2 L \text{ (s}^{-1}\text{)}$		

## II. GLOBAL MODEL (VOLUME-AVERAGED MODEL)

We calculate neutral densities [ $\text{Ar}$  metastables ( $3P_0 + 3P_2$ ) and  $\text{Ar}$  resonants ( $3P_1 + 1P_1$ )], which were notated as  $\text{Ar}^m$  and  $\text{Ar}^r$ , respectively, and charged particle density in the  $\text{Ar}$  plasma maintained in a cylindrical chamber with its inner diameter ( $2R$ ) and length ( $L$ ). The reactions in this model are listed in Table I. The rate coefficients  $k_j (j=1-7)$  are determined from the following equation by the EEPF  $f(\epsilon)$  and the appropriate inelastic cross sections  $Q_j(\epsilon)$  with the threshold energies  $\epsilon_j$ :

$$k_j = (2q/m)^{1/2} \int_{\epsilon_j}^{\infty} Q_j(\epsilon) \epsilon f(\epsilon) d\epsilon / n_e, \quad (1)$$

where  $m$  is the electron mass,  $n_e$  is the electron density,  $q$  is the absolute value of the electron charge, and  $\epsilon$  is the electron energy.

Assumptions for the model are described later.

(i) The EEPF used can be represented as a two-temperature distribution with  $T_e$  and  $T_i$ . The EEPF in the low-energy region below the lowest excitation threshold energy  $\epsilon_1$  ( $\approx 11.6 \text{ V}$ ) is represented by a truncated Maxwellian with temperature  $T_e$ , and in the high-energy region, by a piece of a Maxwellian with temperature  $T_i$ . The EEPF, in which the bulk temperature  $T_e$  is assumed to be equivalent to two-thirds of the average electron energy, is then expressed as follows:<sup>14,15</sup>

$$f(\epsilon) = \begin{cases} \left( \frac{2n_e}{\pi^{1/2} T_e^{3/2}} \right) \exp(-\epsilon/T_e), & (\epsilon < \epsilon_1), \\ \left( \frac{2n_e}{\pi^{1/2} T_e^{3/2}} \right) \exp(-\epsilon/T_i) \exp[-\epsilon_1(1/T_e - 1/T_i)], & (\epsilon > \epsilon_1). \end{cases} \quad (2)$$

(ii) All neutral densities [ $\text{Ar}$ ], [ $\text{Ar}^m$ ], and [ $\text{Ar}^r$ ] have a uniform profile throughout the entire discharge, while the charged particle densities  $n_e$  and [ $\text{Ar}^+$ ] has an inhomogeneous profile in the vicinity of the chamber wall and the skin layer, keeping the charge neutrality  $n_e = [\text{Ar}^+]$  throughout the entire discharge.

(iii) The gas temperature is 400 (K).

Before discussing the rate equations for the neutral and the charged particles as well as the power balance equation, the elucidation for the formation of EEPF structure corresponding to a two-temperature distribution is necessary. Since  $n_e$  and the pressure  $p$  for the plasma of interest are in the ranges of  $10^{16} - 10^{18} \text{ (m}^{-3}\text{)}$  and a few (mTorr)–100 (mTorr), respectively, the e–e Coulomb collision frequency ( $\nu_{ee}$ ) is much larger than the electron energy exchange frequency [ $(m/M)\nu_m$ ] due to the elastic collisions at any  $\epsilon$ . The electrons with very low  $\epsilon$ , which cannot penetrate into the skin layer, are not heated, resulting in a Maxwellian distribution with  $T_i$  by the e–e Coulomb collisions. The electrons with the middle  $\epsilon$  below  $\epsilon_1$ , which can penetrate into the layer, are heated by the joule and stochastic heatings, and transfer their energy to very low energy electrons due to the e–e Coulomb collisions. Thus, the formation of a Maxwellian distribution with  $T_e$  in the middle  $\epsilon$  depends on the energy gain due to the heatings and energy transfer due to the e–e Coulomb collisions with very low energy electrons. The temperature  $T_i$  may come to  $T_e$  with the increase of  $n_e$ , since main e–e collisions are occurred among the electrons with  $\epsilon$  below  $\epsilon_1$  due to the small fraction of the electrons with higher  $\epsilon$  than  $\epsilon_1$ . On the other hand, for the high-energy electrons which can cause the inelastic collisions, the electron energy exchange time due to inelastic collisions corresponding to  $1/\{(2q/m)^{1/2}[\text{Ar}] \sum Q_j(\epsilon) \epsilon^{1/2}\}$  is much shorter than that due to e–e Coulomb collision ( $1/\nu_{ee}$ ), resulting in

the formation of distribution with  $T_i$  which is different from  $T_e$ . Therefore, the EEPF can be represented as a two-temperature distribution with  $T_e$  and  $T_i$ , as used in assumption (i).

The main generation of positive ions is due to the ionization collisions with direct, stepwise and associative ionizations such as metastable–metastable ionization, while the loss of positive ions is due to the wall neutralization. Then, the rate equation for Ar positive ions is given as follows:

$$\frac{d[\text{Ar}^+]}{dt} = (k_6[\text{Ar}^m] + k_7[\text{Ar}^r] + k_5[\text{Ar}])n_e + k_{12}[\text{Ar}^m] \times [\text{Ar}^m] + k_{13}[\text{Ar}^m][\text{Ar}^r] - [\text{Ar}^+]\text{Ar}_{\text{loss}}^+, \quad (3)$$

where the  $k$  values and  $\text{Ar}_{\text{loss}}^+$  are defined in Table I. The ratios  $h_L$  and  $h_R$  of  $n_e$  at the sheath edge where the velocity for Ar positive ion can reach the Bohm velocity  $U_B$  to that at the bulk are given according to the formula by Godyak<sup>16</sup> as

$$h_L = 0.86 \left( 3 + \frac{L}{2\lambda_i} \right)^{-1/2}, \quad (4)$$

$$h_R = 0.80 \left( 4 + \frac{R}{\lambda_i} \right)^{-1/2}, \quad (5)$$

where the ion mean free path  $\lambda_i$  is given by using the total ion-neutral collision cross section  $\sigma_{\text{Ar}} (= 1 \times 10^{-18} \text{ m}^2)$  as  $\lambda_i = 1/([\text{Ar}]\sigma_{\text{Ar}})$ . Here the velocity  $U_B$  is approximately given as  $U_B = (qT_e/M)^{1/2}$  with notation of Ar mass  $M$ .

The dominant generation of the excited neutral densities  $[\text{Ar}^m]$ ,  $[\text{Ar}^r]$  is due to the direct excitation. On the other hand, the metastables interact with Ar resonants and a set of higher levels, which consist of ten levels and are connected optically with the metastables or the resonants, so that their excited neutral species are redistributed through the radiation process from the higher levels produced by the collision between electrons and metastables (or resonants). According to previous articles,<sup>17,18</sup> the rate equations for  $\text{Ar}^m$  and  $\text{Ar}^r$  are given as

$$\begin{aligned} \frac{d[\text{Ar}^m]}{dt} = & k_1[\text{Ar}]n_e + k_{11}[\text{Ar}^r]n_e + \left( \sum_n k_{rh}\delta_{hm}[\text{Ar}^r] \right) n_e \\ & - (k_6n_e[\text{Ar}^m] + k_{12}2[\text{Ar}^m][\text{Ar}^m] + k_{13}[\text{Ar}^m] \\ & \times [\text{Ar}^r] + k_8n_e[\text{Ar}^m]) - \left( \sum_n k_{mh}\delta_{hr} \right) [\text{Ar}^m]n_e \\ & - D_m \left( \frac{1}{\Lambda^2} \right) [\text{Ar}^m], \end{aligned} \quad (6)$$

$$\begin{aligned} \frac{d[\text{Ar}^r]}{dt} = & k_2n_e[\text{Ar}] + k_8n_e[\text{Ar}^m] + \left( \sum_n k_{mh}\delta_{hr} \right) [\text{Ar}^m]n_e \\ & - [\text{Ar}^r](k_7n_e + k_{13}[\text{Ar}^m]) - \left( \sum_n k_{rh}\delta_{hm} \right) \\ & \times [\text{Ar}^r]n_e - [\text{Ar}^r] \left( \frac{1}{\tau} \right). \end{aligned} \quad (7)$$

The power balance equation assumes that the total power  $P_p$  injected into the plasma is dissipated through collision

processes between electrons and neutral species and the kinetic energies of ions and electrons flowing into the walls<sup>4,5,11–13</sup>

$$\begin{aligned} \frac{3}{2} \frac{d(n_e T_e)}{dt} = & \frac{P_p}{q \text{Vol}} - \frac{3m}{M} k_{\text{elas}}[\text{Ar}]n_e T_e - \sum \epsilon_j k_j[\text{Ar}]n_e \\ & - \epsilon_{iz} k_5[\text{Ar}]n_e - (\epsilon_{iz} - \epsilon_1) k_6[\text{Ar}^m]n_e \\ & - (\epsilon_{iz} - \epsilon_1) k_7[\text{Ar}^r]n_e - \text{Ar}_{\text{loss}}^+ \left( 2T_e + V_{\text{sh}} + \frac{T_e}{2} \right), \end{aligned} \quad (8)$$

where  $\epsilon_j$  and  $\epsilon_{iz}$  are the threshold energies of the electronic excitation and ionization, respectively,  $k_{\text{elas}}$  the rate coefficient for the elastic collision and the sheath edge voltage drop  $V_{\text{sh}}$  is given as  $V_{\text{sh}} = (T_e/2) \ln(M/2\pi m)$ .

The Boltzmann equation is introduced to deduce  $T_i$ . Eliminating the energy transfer term from the high-energy electrons to the low-energy electrons due to the inelastic collision and the elastic collision term, for simplicity, the volume-integrated Boltzmann equation for high energy electrons, which can cause the inelastic collisions, can be approximately given as follows:

$$\begin{aligned} \int_{\text{Vol}} d\epsilon \left\{ \frac{[2q\overline{E_\theta^2}(z,r)]\epsilon^{3/2}\nu_{\text{eff}}(\epsilon)}{3m[\omega^2 + \nu_{\text{eff}}^2(\epsilon)]} \frac{d}{d\epsilon} f(\epsilon) \right\} dV \\ = \int_{\text{Vol}} \sum \epsilon^{1/2} \nu_j(\epsilon) f(\epsilon) + \epsilon^{1/2} \nu_i(\epsilon) f(\epsilon) \\ + \epsilon^{1/2} \nu_{\text{esc}}(\epsilon) f(\epsilon) dV, \end{aligned} \quad (9)$$

where  $\overline{E_\theta^2}(z,r)$  is the time-averaged value of the azimuthal rf electric field,  $\omega$  is the rf angular frequency,  $\nu_{\text{eff}}$  is the effective collision frequency corresponding to the sum of the elastic and stochastic collision frequencies, and  $\nu_j(\epsilon)$  and  $\nu_i(\epsilon)$  are the frequencies of the inelastic and ionization collisions. The local EEPF can be given as a function of only  $\epsilon$  from assumption (ii), resulting in the independence of  $\nu_{\text{eff}}(\epsilon)$  on space. Therefore, Eq. (9) can be given as

$$\begin{aligned} \frac{d}{d\epsilon} \left\{ \frac{(2q\overline{E_\theta^2})\epsilon^{3/2}\nu_{\text{eff}}(\epsilon)}{3m[\omega^2 + \nu_{\text{eff}}^2(\epsilon)]} \frac{d}{d\epsilon} f(\epsilon) \right\} \\ = \sum \epsilon^{1/2} \nu_j(\epsilon) f(\epsilon) + \epsilon^{1/2} \nu_i(\epsilon) f(\epsilon) + \epsilon^{1/2} \nu_{\text{esc}}(\epsilon) f(\epsilon), \end{aligned} \quad (10)$$

where the volume-averaged electric field  $\overline{E_\theta^2}$  is given as  $\langle \overline{E_\theta^2} \rangle = \int_{\text{Vol}} \overline{E_\theta^2}(z,r) dV / \text{Vol}$ . On the other hand, integrating the power density  $p_j$  which is given as

$$p_j = [q^2 \overline{E_\theta^2}(z,r) n_e(z,r) \nu_{\text{eff}}] / [m(\nu_{\text{eff}}^2 + \omega^2)]$$

over the entire discharge, the power  $P_p$  can be deduced as

$$P_p = \frac{q^2 \nu_{\text{eff}}}{m(\nu_{\text{eff}}^2 + \omega^2)} \int_0^L \int_{-R}^R n_e(z,r) \overline{E_\theta^2}(z,r) 2\pi r dr dz. \quad (11)$$

Since the injected power  $P_p$  is mainly absorbed within a skin layer of thickness  $\delta$ , the profiles of  $\overline{E_\theta^2}(z,r)$  and  $n_e(z,r)$  are necessary to solve the double integral in Eq. (11). According

to previous articles,<sup>17,18</sup> the profile of  $\overline{E_\theta^2(z,r)}$  is given as  $E_\theta^2(z,r) = E_0^2 \exp(-2z/\delta) J_1^2(3.83r/R)$  using Bessel function  $J_1(3.83r/R)$ . Since the radial profiles of  $E_\theta^2(z,r)$  is obeyed to  $J_1^2(3.83r/R)$ , which has a negligible value near the chamber wall, the assumption of the homogeneous radial density profiles of  $n_e(z,r)$  may not cause the error in calculation of the double integral in Eq. (11). However, the axial profile of  $n_e(z,r)$  must be considered, because the electron density in the skin layer near the sheath is lower than that at the bulk plasma. According to the density profile in one-dimensional planar geometry derived in low pressure discharges,<sup>16</sup> the value of  $n_e(\delta/2,r)$  is approximately given by  $n_e(\delta/2,r) = n_e$  for  $\delta/L \approx 0.2-0.3$ , where  $n_e$  is the bulk electron density. Assuming the axial electron density profile for  $\delta/2 \leq z$  as  $n_e(z,r) = n_e[h_L + (1-h_L)(2z/\delta)]$ , Eq. (11) can be approximately given as

$$P_p \approx \frac{q^2 \nu_{\text{eff}}(0.35h_L + 0.65)n_e}{m(\nu_{\text{eff}}^2 + \omega^2)} \langle \overline{E_\theta^2} \rangle \text{Vol}. \quad (12)$$

Substituting Eq. (12) and relation  $df(\epsilon)/d\epsilon = -f(\epsilon)/T_t$  for the high-energy region into Eq. (10), we obtain

$$\begin{aligned} & \frac{2}{3} \left[ \frac{P_p}{n_e(0.35h_L + 0.65)\text{Vol}q} \right] \left( -\frac{1}{T_t} \right) \frac{d}{d\epsilon} [\epsilon^{3/2} f(\epsilon)] \\ & = \sum_j \nu_j(\epsilon) \epsilon^{1/2} f(\epsilon) + \nu_i(\epsilon) \epsilon^{1/2} f(\epsilon) + \nu_{\text{esc}}(\epsilon) \epsilon^{1/2} f(\epsilon). \end{aligned} \quad (13)$$

Integrating both sides of Eq. (13) over  $\epsilon$  from  $\epsilon_1$  to  $\infty$ , we can obtain

$$T_t = \frac{2}{3q} \left[ \frac{P_p}{n_e(0.35h_L + 0.65)\text{Vol}} \right] \frac{\epsilon_1^{3/2} f(\epsilon_1)}{n_e(\sum_j \nu_j + \nu_i + \nu_{\text{esc}})}. \quad (14)$$

Here we can approximate that  $\nu_{\text{esc}}$  is equal to  $\nu_i$  due to the balance between the generation and the loss of charged particles. To estimate the inelastic collision frequencies  $\nu_j$  ( $=k_j[\text{Ar}]$ ) and  $\nu_i$  ( $=k_i[\text{Ar}]$ ) from Eq. (1) in a simple way, the cross sections  $Q_j(\epsilon)$  for various inelastic collisions are approximated by the following analytical expression:<sup>14</sup>

$$Q_j(\epsilon) = \begin{cases} q_j(1 - \epsilon_j/\epsilon) & \epsilon > \epsilon_j \\ 0 & \epsilon \leq \epsilon_j. \end{cases} \quad (15)$$

From Eqs. (1), (2), and (15), the rate coefficients  $k_j$  for inelastic collisions are given in terms of  $T_e$  and  $T_t$ :

$$k_j = 2 \left( \frac{2q}{\pi m} \right)^{1/2} q_j \left( \frac{T_t}{T_e} \right)^2 \sqrt{T_e} e^{-\epsilon_1/T_e} e^{-(\epsilon_j - \epsilon_1)/T_t}. \quad (16)$$

Substituting Eq. (16) into Eq. (14), the following equation can be obtained:

$$\begin{aligned} T_t^3 &= \frac{2}{3q} \left\{ \frac{P_p}{n_e(0.35h_L + 0.65)\text{Vol}[\text{Ar}]} \right\} \left( \frac{m_e}{2q} \right)^{1/2} \\ &\times \left\{ \frac{\epsilon_1^{3/2}}{\sum q_j \exp[-(\epsilon_j - \epsilon_1)/T_t] + 2q_i \exp[-(\epsilon_i - \epsilon_1)/T_t]} \right\}. \end{aligned} \quad (17)$$

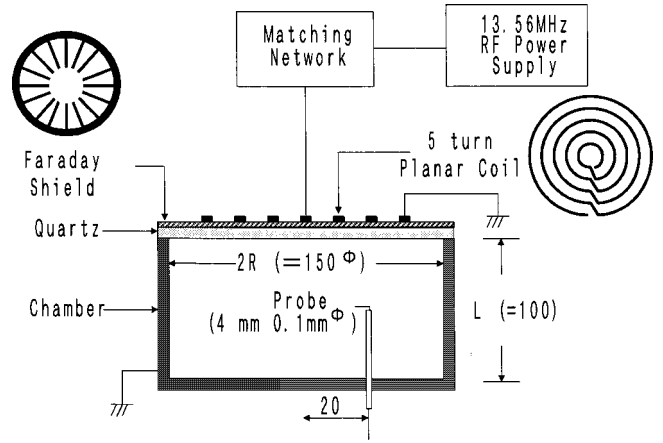


FIG. 1. Schematic diagram of experimental apparatus.

Together with Eqs. (17), Eqs. (3) and (6)–(8) are solved as the time evolution of neutral and charged particle densities and electron energy by the Runge–Kutta method. When the time variations in these quantities disappear, the calculated values correspond to solutions for the steady state.

### III. EXPERIMENTAL APPARATUS

A schematic diagram of the experimental apparatus is shown in Fig. 1. The chamber was cylindrical, 15 cm in inner diameter and 10 cm in length, and a quartz plate of 1.0 cm thickness was placed at the upper end of the chamber. The discharge was sustained in the stainless steel chamber with the quartz plate, by the azimuthal electric field induced by the rf coil current supplied to a planar five-turn coil from the power source connected to an L-type capacitive matching network. The planar coil mounted at about 0.4 cm above the quartz plate was concentric in the center of the chamber to maintain the discharge symmetry. An electrostatic shield practically eliminated the capacitive coupling between the coil and the plasma, resulting in suppression of the rf plasma potential fluctuation. A cylindrical probe of 4 mm in length and 0.1 mm in diameter was installed at a radial position 2.0 cm from the chamber center. The power  $P_p$  injected into the plasma was estimated by subtracting the transmitted power without plasma from that with plasma at the same current.

The EEDF  $F(\epsilon)$  was measured by detecting the second derivative  $i_p''$  of the probe current  $i_p$  with respect to the probe bias voltage  $V_p$ , according to the Druyvesteyn formula<sup>23</sup>

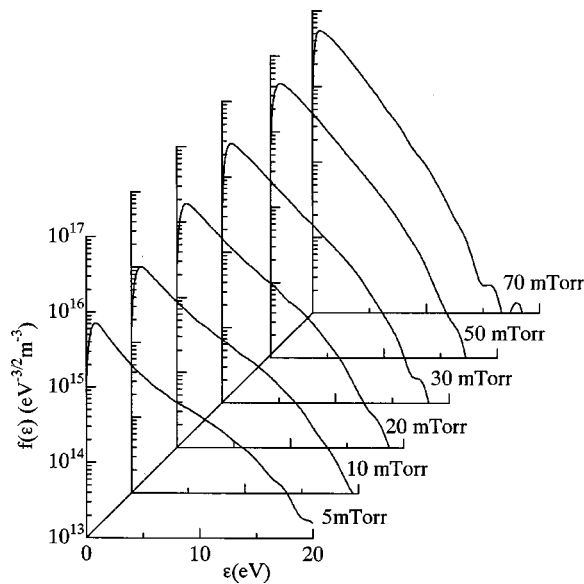
$$F(\epsilon) = \frac{4}{(Aq^2n_e)} \left( \frac{m}{2q} \right)^{1/2} V^{1/2} i_p'', \quad (18)$$

where  $\epsilon$  is in electron volts,  $A$  is the probe area, and  $V$  is the difference between the plasma potential  $V_s$ , which is determined as  $V_p$  corresponding to  $i_p''=0$ , and  $V_p$ . The EEPF  $f(\epsilon)$  measured can be then deduced as

$$f(\epsilon) = F(\epsilon) \epsilon^{-1/2}. \quad (19)$$

The EEDF detection system is described in a previously published article.<sup>5</sup>

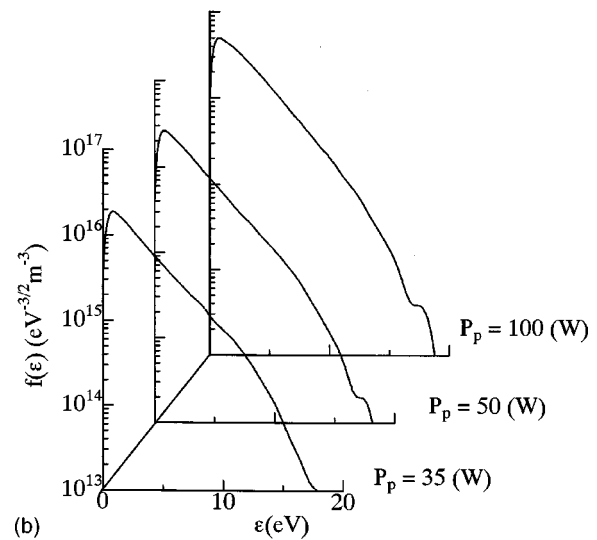
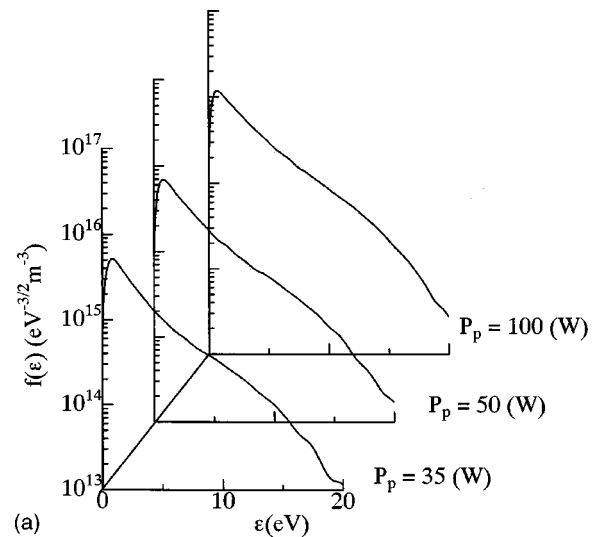


FIG. 2. EEPF  $f(\epsilon)$  measured for various pressures, where  $P_p = 50$  W.

#### IV. RESULTS AND DISCUSSION

Pressure dependences of the EEPF  $f(\epsilon)$  measured for  $P_p = 50$  W are shown in Fig. 2. The electron behavior can be regarded as the nonlocal kinetics in our experimental pressure range, because the electron energy relaxation length at any electron energy is larger than at least  $L/2$ . The EEPF structure measured at  $p = 5$  mTorr can be rather interpreted as a “three-temperature” distribution due to depletion of high-energy electrons at the threshold between the lowest excitation and ionization energy. The bi-Maxwellian distribution structure below the lowest excitation threshold energy is not so prominent compared with the previous results<sup>2</sup> for low pressure Ar due to high  $n_e$ . The EEPFs at  $p$  higher than 10 mTorr can be approximated using the two-temperature  $T_e$  and  $T_i$ , since such EEPFs include depletion at energy higher than the lowest excitation threshold energy. The relation  $\nu_{ee} \leq \nu_j$  means that the slope of the EEPF tail at  $p$  higher than 10 mTorr is determined by the inelastic collision rather than the e-e collision, resulting in the difference in slope corresponding to  $T_e$  and  $T_i$ . Typical power dependences of EEPF at  $p = 5$  mTorr and  $p = 30$  mTorr are also shown in Figs. 3(a) and 3(b). As shown in Fig. 3(a), the bi-Maxwellian distribution structure in the low-energy range disappears gradually, since the electron energy relaxation due to e-e collision is more dominant with increasing  $n_e$ . On the other hand, the EEPF structure in the low-energy region at  $p$  higher than 10 mTorr tends to form a Maxwellian-like distribution and does not depend on  $P_p$  strongly. Therefore, these experimental results show that the two-temperature approximation of EEPF is valid in the wide ranges of  $p$  and  $P_p$ .

Theoretical and experimental pressure dependences of  $n_e$ ,  $T_e$ ,  $T_i$ , and  $V_s$  for  $P_p = 50$  W are shown in Figs. 4(a)–4(c) together with the theoretical pressure dependence of densities of the excited species in Fig. 4(d). The measured  $n_e$  is given as  $n_e = (2/q)^{3/2} (m^{1/2}/A) \int_0^\infty V^{1/2} i_p'' dV$  and the temperatures  $T_e$  and  $T_i$  were determined from the slope of EEPF at  $\epsilon$  around 4–8 eV and  $\epsilon$  around 12–15 eV, respectively,

FIG. 3. Power dependences of EEPF for  $p = 5$  mTorr in (a) and  $p = 30$  mTorr in (b).

while the theoretical  $V_s$  is given as  $V_s = V_{sh} + T_e/2$ . The measured and calculated densities  $n_e$  increase as the pressure increases, while the temperatures  $T_e$  and  $T_i$  decrease, resulting in the decrease of  $V_s$ . The temperatures  $T_e$  and  $T_i$  are mainly determined by the charged particle balance and the balance for the high energy electrons, respectively. The decrease of the wall loss of the charged particles and the increase of the step ionization frequency with the increase of  $p$  may cause the decrease of the direct ionization frequency, resulting in the decrease of  $T_e$  and  $T_i$ . Therefore, the density  $n_e$ , which is determined by the power balance, increases with  $p$  under the condition of the constant  $P_p$ . The  $p$  dependence of the measured and calculated  $n_e$  can be given as asymptotes by two-straight lines. The slope at pressure higher than 20–30 mTorr is considerably larger than that at pressure lower than 20 mTorr, because the step ionization related to the metastables and the resonants is more dominant compared with the direct ionization. In calculation, the ratio of the step ionization frequency to the total ionization fre-

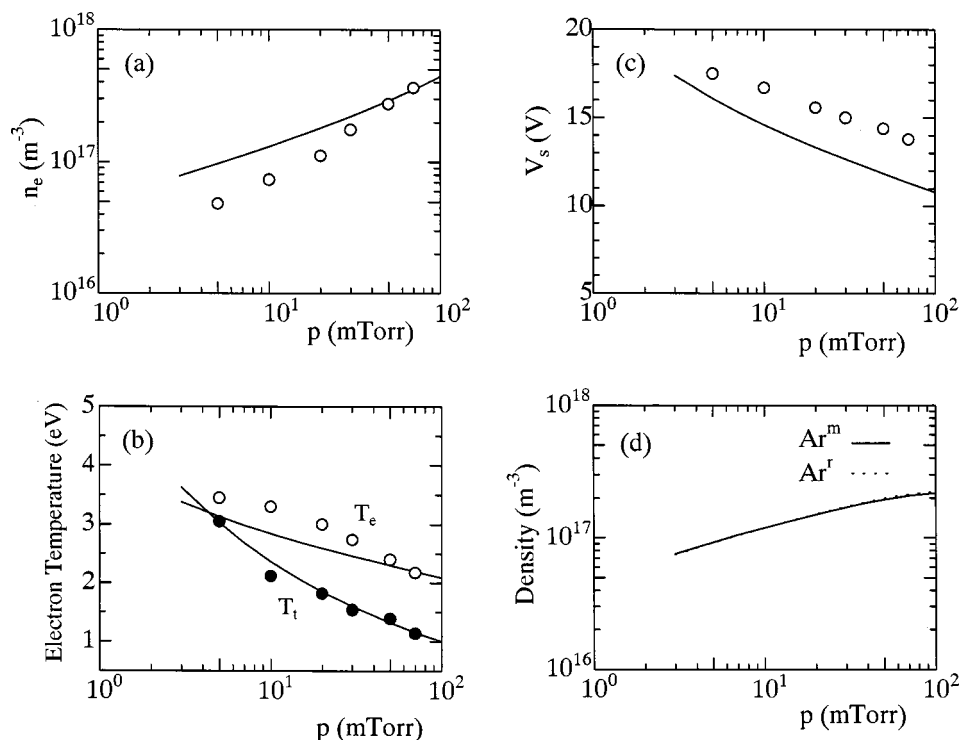


FIG. 4. Theoretical and experimental pressure-dependences of  $n_e$  in (a), the temperatures  $T_e$  (eV) and  $T_i$  (eV) in (b),  $V_s$  in (c) and calculated densities of the excited species in (d).

quency changes from 20% to 80% with increase of  $p$ . As shown in Fig. 4, the discrepancy between theoretical and experimental  $n_e$ ,  $T_e$  for  $p \leq 10$  mTorr remains, while good agreement between theoretical and experimental  $T_i$  is obtained at any pressure. The difference between the theoretical and experimental  $V_s$  is mainly caused by the difference between theoretical and experimental  $T_e$ . The discrepancy for  $p \leq 10$  mTorr may be caused by the accuracy of the two-temperature approximation of the EEPF. The assumption that the effect of the energy relaxation due to the e-e collisions induces the formation of a single Maxwellian distribution in the low-energy region is used in the model. To satisfy such an assumption, the density  $n_e$  is required to be higher than  $10^{17} \text{ m}^{-3}$  under the condition of  $p$  lower than 10 mTorr in the experiment. Strictly speaking, the description including the formation of a bi-Maxwellian distribution in the bulk region, which means the three-temperature approximation of EEPF, are necessary in the case of  $n_e$  lower than  $10^{17} \text{ m}^{-3}$ . In addition, the shift of the knee point of the measured EEPF from the lowest excitation threshold energy at  $p$  lower than 10 mTorr may cause the difference between the theoretical and experimental results. The treatment of the three-temperature approximation of the EEPF and the precise determination of the knee point at low  $p$  are out of scope in the present article.

Theoretical power-dependence of  $n_e$  for various  $p$  is shown in Fig. 5. As shown in Fig. 5, the density  $n_e$  increases linearly with  $P_p$  at low pressure, while the linear relation between  $n_e$  and  $P_p$  does not hold as  $p$  increases. The temperatures  $T_e$  and  $T_i$  decrease slightly with the increase of  $P_p$  from  $T_e = 2.75 \text{ eV}$  ( $T_i = 2.11 \text{ eV}$ ) to  $T_e = 2.60 \text{ eV}$  ( $T_i = 2.00 \text{ eV}$ ) for 15 mTorr,  $T_e = 2.55 \text{ eV}$  ( $T_i = 1.65 \text{ eV}$ ) to  $T_e = 2.37 \text{ eV}$  ( $T_i = 1.53 \text{ eV}$ ) for 30 mTorr and  $T_e = 2.32 \text{ eV}$  ( $T_i = 1.25 \text{ eV}$ ) to  $T_e = 2.10 \text{ eV}$  ( $T_i = 1.08 \text{ eV}$ ) for 70 mTorr be-

cause of the increase of the step ionization frequency. The weak dependences of  $T_e$  and  $T_i$  on  $P_p$  can cause the shift of the linear relationship between  $n_e$  and  $P_p$ .

## V. CONCLUDING REMARKS

The EEPF is measured with a Langmuir probe in inductively coupled rf (13.56 MHz) Ar discharges over a pressure range from 5 to 70 mTorr.

The EEPF structure measured at  $p = 5$  mTorr can be interpreted as a three-temperature distribution due to the depletion of high-energy electrons at the threshold between the excitation and ionization energy, although the bi-Maxwellian distribution structure in the energy region below the lowest excitation threshold energy is not prominent. A change in

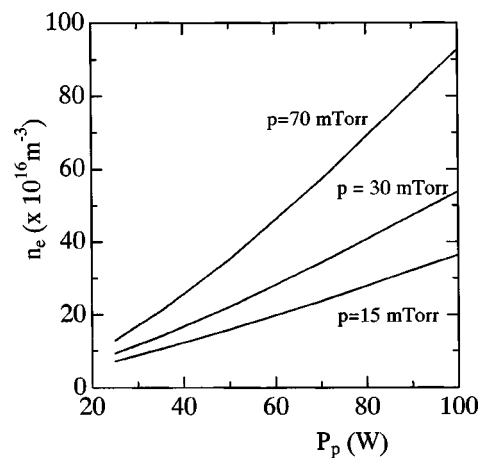


FIG. 5. Theoretical power dependence of  $n_e$  for various  $p$ .

EEPF structure with increase of pressure are observed, and the EEPFs measured at the pressure higher 10 mTorr can be approximated by two temperatures.

A global model using two-temperature approximation is proposed and compared with the experimental results. The model consists of the rate equations for neutrals and charged particle and an energy-balance equation for electrons, including the balance equation for the high-energy electrons to deduce the tail temperature. Pressure dependences of the electron density and temperatures predicted in this global model agree with the experimental results especially in the ranges of pressure higher than 10 mTorr.

## ACKNOWLEDGMENTS

We are grateful to Professor A. J. Lichtenberg of the University of California at Berkeley for continuous discussions. This work was supported by a Grant-in-Aid for Science Research from the Ministry of Education, Science, Sports, and Culture in Japan.

<sup>1</sup>V. A. Godyak, R. B. Piejak, and B. M. Alexandrovich, *Plasma Sources Sci. Technol.* **4**, 332 (1995).

<sup>2</sup>V. A. Godyak and V. I. Kolobov, *Phys. Rev. Lett.* **81**, 369 (1998).

<sup>3</sup>M. S. Barnes, J. C. Forster, and J. H. Keller, *Appl. Phys. Lett.* **62**, 2622 (1993).

<sup>4</sup>J. T. Gudmundsson, T. Kimura, and M. A. Lieberman, *Plasma Sources Sci. Technol.* **8**, 22 (1999).

<sup>5</sup>T. Kimura and K. Ohe, *Plasma Sources Sci. Technol.* **8**, 553 (1999).

<sup>6</sup>M. J. Kushner, *J. Appl. Phys.* **54**, 4958 (1983).

<sup>7</sup>M. Surendra and D. B. Graves, *IEEE Trans. Plasma Sci.* **19**, 144 (1991).

<sup>8</sup>R. S. Wise, P. Lymberopoulos, and D. J. Economou, *Appl. Phys. Lett.* **68**, 2499 (1996).

<sup>9</sup>U. Kortshagen, I. Pukropski, and L. D. Tsendin, *Phys. Rev. E* **51**, 6063 (1995).

<sup>10</sup>U. Kortshagen, C. Busch, and L. D. Tsendin, *Plasma Sources Sci. Technol.* **5**, 1 (1996).

<sup>11</sup>S. Ashida, C. Lee, and M. A. Lieberman, *J. Vac. Sci. Technol. A* **13**, 2498 (1995).

<sup>12</sup>C. Lee, D. B. Graves, M. A. Lieberman, and D. W. Hess, *J. Electrochem. Soc.* **141**, 1546 (1994).

<sup>13</sup>C. Lee and M. A. Lieberman, *J. Vac. Sci. Technol. A* **13**, 368 (1995).

<sup>14</sup>R. W. Callis and D. T. Tuma, *IEEE Trans. Plasma Sci.* **2**, 283 (1974).

<sup>15</sup>K. Wani, *J. Appl. Phys.* **63**, 5683 (1988).

<sup>16</sup>V. A. Godyak, *Soviet Radio Frequency Discharge Research* (Delphic Falls Church, VA, 1986).

<sup>17</sup>J. Hopwood, C. R. Guarnieri, S. J. Whitehair, and J. J. Cuomo, *J. Vac. Sci. Technol. A* **11**, 152 (1993).

<sup>18</sup>V. Vahedi, M. A. Lieberman, G. DiPeso, T. D. Rognlien, and D. Hewett, *J. Appl. Phys.* **78**, 1446 (1995).

<sup>19</sup>C. M. Ferreira and J. Loureiro, *J. Appl. Phys.* **57**, 82 (1985).

<sup>20</sup>N. L. Bassett and D. J. Economou, *J. Appl. Phys.* **75**, 1931 (1994).

<sup>21</sup>M. Hayashi (private communication).

<sup>22</sup>D. Ton-That and M. R. Flannery, *Phys. Rev. A* **15**, 517 (1977).

<sup>23</sup>M. J. Druryvesteyn, *Z. Phys.* **64**, 790 (1930).